Defects in carbon implanted silicon calculated by classical potentials and first-principles methods

F. Zirkelbach,[1] B. Stritzker,[1] K. Nordlund,[2] J. K. N. Lindner,[3] W. G. Schmidt,[3] and E. Rauls[3]

[1]*Experimentalphysik IV, Universität Augsburg, 86135 Augsburg, Germany*
[2]*Department of Physics, University of Helsinki, 00014 Helsinki, Finland*
[3]*Department Physik, Universität Paderborn, 33095 Paderborn, Germany*

A comparative theoretical investigation of carbon interstitials in silicon is presented. Calculations using classical potentials are compared to first-principles density-functional theory calculations of the geometries, formation, and activation energies of the carbon dumbbell interstitial, showing the importance of a quantum-mechanical description of this system. In contrast to previous studies, the present first-principles calculations of the interstitial carbon migration path yield an activation energy that excellently matches the experiment. The bond-centered interstitial configuration shows a net magnetization of two electrons, illustrating the need for spin-polarized calculations.

I. INTRODUCTION

Silicon carbide (SiC) has a number of remarkable physical and chemical properties. The wide band-gap semiconductor (2.3–3.3 eV) exhibiting a high breakdown field, saturated electron drift velocity, and thermal conductivity in conjunction with its unique thermal and mechanical stability as well as radiation hardness is a suitable material for high-temperature, high-frequency, and high-power devices,[1,2] which are moreover deployable in harsh and radiation-hard environments.[3] SiC, which forms fourfold coordinated mostly covalent bonds, tends to crystallize into many different modifications, which solely differ in the one-dimensional stacking sequence of identical, close-packed SiC bilayers.[4] Different polytypes exhibit different properties, in which the cubic phase of SiC (3C-SiC) shows increased values for the thermal conductivity and breakdown field compared to other polytypes,[1] which is, thus, most effective for high-performance electronic devices.

Thin films of 3C-SiC can be fabricated by chemical vapor deposition and molecular beam epitaxy on hexagonal SiC (Refs. 5–7) and Si (Refs. 7–10) substrates. Next to these methods, high-dose carbon implantation into crystalline silicon (c-Si) with subsequent or *in situ* annealing was found to result in SiC microcrystallites in Si.[11] Ion-beam synthesis (IBS) has become a promising method to form thin SiC layers of high quality exclusively of the 3C polytype embedded in and epitactically aligned to the Si host featuring a sharp interface.[12–14] However, only little is known about the SiC conversion in C implanted Si. High-resolution transmission electron microscopy (HREM) studies[15–17] suggest the formation of C-Si dimers (dumbbells) on regular Si lattice sites, which agglomerate into large clusters indicated by dark contrasts and otherwise undisturbed Si lattice fringes in HREM. Once a critical radius of 2–4 nm is reached, a topotactic transformation into a 3C-SiC precipitate occurs. The transformation is manifested by the disappearance of dark contrasts in favor of Moiré patterns due to the lattice mismatch of 20% of the 3C-SiC precipitate and c-Si. The insignificantly lower Si density of SiC ($\approx 4\%$) compared to c-Si results in the emission of only a few excess Si atoms. A de-

tailed understanding of the underlying processes will enable significant technological progress in 3C-SiC thin-film formation and likewise offer perspectives for processes which rely upon prevention of precipitation events, e.g., the fabrication of strained pseudomorphic $Si_{1-y}C_y$ heterostructures.[18,19]

Atomistic simulations offer a powerful tool to study materials on a microscopic level providing detailed insight not accessible by experiment. Relevant structures consisting of $\approx 10^4$ atoms for the nanocrystal and even more atoms for a reasonably sized Si host matrix are too large to be completely described by high-accuracy quantum-mechanical methods. Directly modeling the dynamics of the processes mentioned above almost inevitably requires the atomic interaction to be described by less accurate though computationally more efficient classical potentials. The most common empirical potentials for covalent systems are the Stillinger-Weber[20] (SW), Brenner,[21] Tersoff,[22] and environment-dependent interatomic potential.[23–25] Until recently,[26] a parametrization to describe the C-Si multicomponent system within the mentioned interaction models did only exist for the Tersoff[27] and related potentials, e.g., the one by Gao and Weber.[28] Whether such potentials are appropriate for the description of the physical problem has, however, to be verified first by applying classical and quantum-mechanical methods to relevant processes that can be treated by both methods. For instance, a comparison of empirical potential molecular dynamics (MD) and density-functional theory (DFT) calculations showed that SW is best suited for simulations of dislocation nucleation processes[29] and threshold displacement energy calculations[30] in Si important in ion implantation while the Tersoff potential yielded a qualitative agreement for the interaction of Si self-interstitials with substitutional C.[31] Antisite pairs and defects in SiC have been investigated, both classically[32,33] employing the Gao/Weber potential[28] and quantum mechanically,[34–37] which, both, agree very well with experimental results.[38–40] An extensive comparison[41] concludes that each potential has its strengths and limitations and none of them is clearly superior to others. Despite their shortcomings these potentials are assumed to be reliable for large-scale simulations[29,41,42] on specific problems under investigation providing insight into phenomena that are otherwise not accessible by experimental or first-

TABLE I. Formation energies of carbon point defects in crystalline silicon determined by classical potential and *ab initio* methods. The formation energies are given in electron volt. T denotes the tetrahedral, H the hexagonal, and BC the bond-centered interstitial configuration. S corresponds to substitutional C. Formation energies for unstable configurations obtained by classical potential MD are marked by an asterisk and determined by using the low kinetic-energy configuration shortly before the relaxation into the more favorable configuration starts.

	T	H	$\langle 1\ 0\ 0 \rangle$ dumbbell	$\langle 1\ 1\ 0 \rangle$ dumbbell	S	BC
Erhart/Albe	6.09	9.05*	3.88	5.18	0.75	5.59*
VASP	Unstable	Unstable	3.72	4.16	1.95	4.66
Tersoff[a]	3.8	6.7	4.6	5.9	1.6	5.3
Ab initio[b,c]			x		1.89[b]	$x+2.1$ [c]

[a]Reference 56.
[b]Reference 57.
[c]Reference 58.

principles methods. Remaining shortcomings have frequently been resolved by modifying the interaction[43–45] or extending it[46] with data gained from *ab initio* calculations.[47]

In this work, the applicability of a Tersoff-type bond-order potential[48] to basic processes involved in the initially mentioned SiC precipitation mechanism has been investigated by comparing results gained by classical and *ab initio* calculations. In the following, a comparative investigation of density-functional theory studies and classical potential calculations of the structure, energetics, and mobility of carbon defects in silicon is presented.

II. METHODOLOGY

The first-principles DFT calculations have been performed with the plane-wave-based Vienna *ab initio* simulation package (VASP).[49] The Kohn-Sham equations were solved using the generalized-gradient exchange-correlation functional approximation proposed by Perdew and Wang.[50,51] The electron-ion interaction is described by norm-conserving ultrasoft pseudopotentials[52] as implemented in VASP.[53] Throughout this work, an energy cutoff of 300 eV was used to expand the wave functions into the plane-wave basis. Sampling of the Brillouin zone was restricted to the Γ point. Some test calculations were performed with a $(2 \times 2 \times 2)$ k-point set. The defect structures and the migration paths have been modeled in cubic supercells containing 216 Si atoms. The ions and cell shape were allowed to change in order to realize a constant pressure simulation. Spin polarization has been fully accounted for.

For the classical potential calculations, a supercell of nine Si lattice constants in each direction consisting of 5832 Si atoms has been used. A Tersoff-type bond-order potential by Erhart and Albe (EA) (Ref. 48) has been utilized, which accounts for nearest-neighbor interactions only realized by a cut-off function dropping the interaction to zero in between the first and second next-neighbor distance. The potential was used as is, i.e., without any repulsive potential extension at short interatomic distances. Constant pressure simulations are realized by the Berendsen barostat[54] using a time constant of 100 fs and a bulk modulus of 100 GPa for Si. Structural relaxation in the MD run is achieved by the velocity

Verlet algorithm[55] and the Berendsen thermostat[54] with a time constant of 100 fs and the temperature set to 0 K. Additionally, a time constant of 1 fs resulting in direct velocity scaling was used for relaxation within the mobility calculations. A fixed time step of 1 fs for integrating the equations of motion was used.

III. RESULTS

According to the assumed SiC precipitation model described in Sec. I, carbon interstitial defects form and agglomerate into large clusters. Thus, it is of crucial importance to investigate the various possible structures of carbon defects and the mobility of the lowest energy, hence most probable, defect configuration in crystalline silicon.

A. Carbon interstitials in various geometries

Table I summarizes the formation energies of defect structures for the EA and DFT calculations performed in this work as well as further results from literature. The formation energy $E - N_{Si}\mu_{Si} - N_C\mu_C$ is defined in the same way as in the articles used for comparison[56,57] choosing SiC as a reservoir for the carbon impurity in order to determine μ_C. Relaxed geometries are displayed in Fig. 1.

Substitutional carbon (C_{sub}) occupying an already vacant Si lattice site, which is in fact not an interstitial defect, is found to be the lowest configuration with regard to energy for all potential models. DFT calculations performed in this work are in good agreement with results obtained by classical potential simulations by Tersoff[56] and *ab initio* calculations done by Dal Pino *et al.*[57] However, the EA potential dramatically underestimates the C_{sub} formation energy, which is a definite drawback of the potential.

Except for the Tersoff potential, the $\langle 1\ 0\ 0 \rangle$ dumbbell (C_i) is the energetically most favorable interstitial configuration, in which the C and Si dumbbell atoms share a Si lattice site. This finding is in agreement with several theoretical[57–60] and experimental[61,62] investigations. Tersoff as well, considers C_i to be the ground-state configuration and believes an artifact due to the abrupt C-Si cutoff used in the potential to be responsible for the small value of the tetrahedral forma-
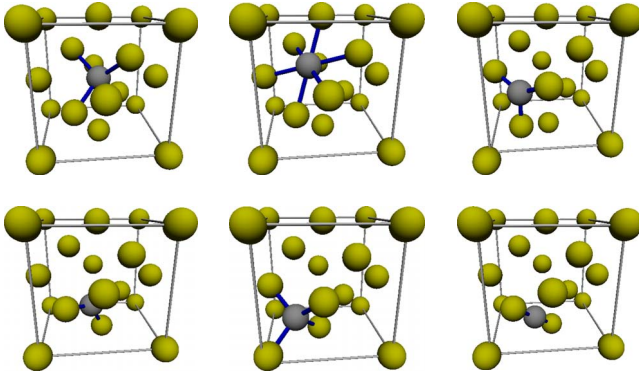
FIG. 1. (Color online) Configurations of carbon point defects in silicon. The silicon/carbon atoms and the bonds (only for the interstitial atom) are illustrated by yellow/gray spheres and blue lines. Bonds are drawn for atoms located within a certain distance and do not necessarily correspond to chemical bonds.

tion energy.[56] It should be noted that EA and DFT predict almost equal formation energies. However, there is a qualitative difference while the C-Si distance of the dumbbell atoms is almost equal for both methods, the position along $[0\ 0\ 1]$ of the dumbbell inside the tetrahedron spanned by the four next-neighbored Si atoms differs significantly. The dumbbell based on the EA potential is almost centered around the regular Si lattice site as can be seen in Fig. 1 whereas for DFT calculations, it is translated upward with the C atom forming an almost collinear bond to the two Si atoms of the top face of the tetrahedron and the bond angle of the Si dumbbell atom to the two bottom face Si atoms approaching 120°. This indicates predominant sp and sp^2 hybridization for the C and Si dumbbell atom, respectively. Obviously the classical potential is not able to reproduce the clearly quantum mechanically dominated character of bonding.

Both, EA and DFT reveal the hexagonal configuration unstable relaxing into the C_i ground-state structure. Tersoff finds this configuration stable, though it is the most unfavorable. Thus, the highest formation energy observed by the EA potential is the tetrahedral configuration, which turns out to be unstable in DFT calculations. The high formation energy of this defect involving a low probability to find such a defect in classical potential MD acts in concert with finding it unstable by the more accurate quantum-mechanical description.

The $\langle 1\ 1\ 0 \rangle$ dumbbell constitutes the second most favorable configuration, reproduced by both methods. It is followed by the bond-centered (BC) configuration. However, even though EA yields the same difference in energy with respect to the $\langle 1\ 1\ 0 \rangle$ defect as DFT does, the BC configuration is found to be a saddle point within the EA description relaxing into the $\langle 1\ 1\ 0 \rangle$ configuration. Tersoff indeed predicts a metastable BC configuration. However, it is not in the correct order and lower in energy than the $\langle 1\ 1\ 0 \rangle$ dumbbell. Please note, that Capaz *et al.*[58] in turn found this configuration to be a saddle point, which is about 2.1 eV higher in energy than the C_i configuration. This is assumed to be due to the neglection of the electron spin in these calculations. Another DFT calculation without fully accounting for

the electron spin results in the smearing of a single electron over two nondegenerate states for the BC configuration. This problem is resolved by spin-polarized calculations resulting in a net spin of one accompanied by a reduction in the total energy by 0.3 eV and the transformation into a metastable local minimum configuration. All other configurations are not affected.

To conclude, we observed discrepancies between the results from classical potential calculations and those obtained from first principles. Within the classical potentials, EA outperforms Tersoff and is, therefore, used for further comparative studies. Both methods (EA and DFT) predict the $\langle 1\ 0\ 0 \rangle$ dumbbell interstitial configuration to be most stable. Also the remaining defects and their relative energies are described fairly well. It is thus concluded that—so far— modeling of the SiC precipitation by the EA potential might lead to trustable results.

B. Mobility

A measure for the mobility of the interstitial carbon is the activation energy for the migration path from one stable position to another. The stable defect geometries have been discussed in the previous section. In the following, the migration of the most stable configuration, i.e., C_i, from one site of the Si host lattice to a neighboring site has been investigated by both, EA and DFT calculations utilizing the constraint conjugate gradient relaxation technique.[63] Three migration pathways are investigated. The starting configuration for all pathways was the $[0\ 0\ \bar{1}]$ dumbbell interstitial configuration. In path 1 and 2, the final configuration is a $[0\ 0\ 1]$ and $[0\ \bar{1}\ 0]$ dumbbell interstitial, respectively, located at the next-neighbored Si lattice site displaced by $\frac{a_{Si}}{4}[1\ 1\ \bar{1}]$, where a_{Si} is the Si lattice constant. In path 1, the C atom resides in the $(1\ 1\ 0)$ plane crossing the BC configuration whereas in path 2, the C atom moves out of the $(1\ 1\ 0)$ plane. Path 3 ends in a $[0\ \bar{1}\ 0]$ configuration at the initial lattice site and, for this reason, corresponds to a reorientation of the dumbbell, a process not contributing to long-range diffusion.

The lowest-energy path (path 2) as detected by the first-principles approach is illustrated in Fig. 2, in which the $[0\ 0\ \bar{1}]$ dumbbell migrates toward the next-neighbored Si atom escaping the (110) plane forming a $[0\ \bar{1}\ 0]$ dumbbell. The activation energy of 0.9 eV excellently agrees with experimental findings ranging from 0.70 to 0.87 eV.[62,64,65]

Calculations based on the EA potential yield a different picture. Figure 3 shows the evolution of structure and energy along the lowest-energy migration path (path 1) based on the EA potential. Due to symmetry, it is sufficient to merely consider the migration from the BC to the C_i configuration. Two different pathways are obtained for different time constants of the Berendsen thermostat. With a time constant of 1 fs, the C atom resides in the $(1\ 1\ 0)$ plane resulting in a migration barrier of 2.4 eV. However, weaker coupling to the heat bath realized by an increase in the time constant to 100 fs enables the C atom to move out of the $(1\ 1\ 0)$ plane already at the beginning, which is accompanied by a reduction in energy, approaching the final configuration on a
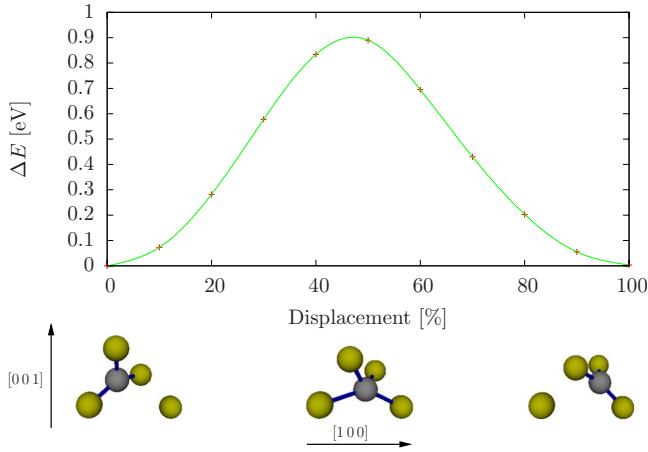
FIG. 2. (Color online) Migration barrier and structures of the $[0\ 0\ \bar{1}]$ dumbbell (left) to the $[0\ \bar{1}\ 0]$ dumbbell (right) transition as obtained by first-principles methods. The activation energy of 0.9 eV agrees well with experimental findings of 0.70 eV (Ref. 64), 0.73 eV (Ref. 62), and 0.87 eV (Ref. 65).

curved path. The energy barrier of this path is 0.2 eV lower in energy than the direct migration within the (1 1 0) plane. It should be noted that the BC configuration is actually not a local minimum configuration in EA-based calculations since a relaxation into the $\langle 1\ 1\ 0 \rangle$ dumbbell configuration occurs. However, investigating further migration pathways involving the $\langle 1\ 1\ 0 \rangle$ interstitial did not yield lower migration barriers. Thus, the activation energy should at least amount to 2.2 eV.
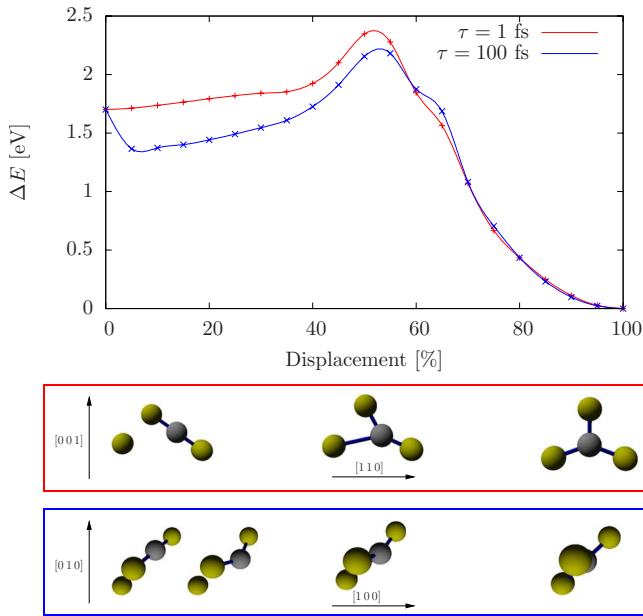
FIG. 3. (Color online) Migration barrier and structures of the bond-centered (left) to $[0\ 0\ \bar{1}]$ dumbbell (right) transition utilizing the classical potential method. Two different pathways are obtained for different time constants of the Berendsen thermostat. The lowest activation energy is 2.2 eV.

IV. DISCUSSION

The first-principles results are in good agreement to previous work on this subject.[57–60] The C-Si $\langle 1\ 0\ 0 \rangle$ dumbbell interstitial is found to be the ground-state configuration of a C defect in Si. The lowest migration path already proposed by Capaz *et al.*[58] is reinforced by an additional improvement of the quantitative conformance of the barrier height calculated in this work (0.9 eV) with experimentally observed values (0.70–0.87 eV).[62,64,65] However, it turns out that the bond-centered configuration is not a saddle-point configuration as proposed by Capaz *et al.*[58] but constitutes a real local minimum if the electron spin is properly accounted for. A net magnetization of two electrons, which is already clear by simple molecular orbital theory considerations on the bonding of the *sp*-hybridized C atom, is settled. By investigating the charge-density isosurface, it turns out that the two resulting spin-up electrons are localized in a torus around the C atom. With an activation energy of 0.9 eV, the C_i carbon interstitial can be expected to be highly mobile at prevailing temperatures in the process under investigation, i.e., IBS.

We found that the description of the same processes fails if classical potential methods are used. Already the geometry of the most stable dumbbell configuration differs considerably from that obtained by first-principles calculations. The classical approach is unable to reproduce the correct character of bonding due to the deficiency of quantum-mechanical effects in the potential. Nevertheless, both methods predict the same type of interstitial as the ground-state configuration. Furthermore, the relative energies of the other defects are reproduced fairly well. From this, a description of defect structures by classical potentials looks promising. However, focusing on the description of diffusion processes the situation has changed completely. Qualitative and quantitative differences exist. First of all, a different pathway is suggested as the lowest-energy path, which again might be attributed to the absence of quantum-mechanical effects in the classical interaction model. Second, the activation energy is overestimated by a factor of 2.4 compared to the more accurate quantum-mechanical methods and experimental findings. This is attributed to the sharp cutoff of the short-range potential. As already pointed out in a previous study,[45] the short cutoff is responsible for overestimated and unphysical high forces of next-neighbor atoms. The overestimated migration barrier, however, affects the diffusion behavior of the C interstitials. By this artifact, the mobility of the C atoms is tremendously decreased resulting in an inaccurate description or even absence of the dumbbell agglomeration as proposed by the precipitation model.

V. SUMMARY

To conclude, we have shown that *ab initio* calculations on interstitial carbon in silicon are very close to the results expected from experimental data. The calculations presented in this work agree well with other theoretical results. So far, the best quantitative agreement with experimental findings has

been achieved concerning the interstitial carbon mobility. We have shown that the bond-centered configuration indeed constitutes a real local minimum configuration resulting in a net magnetization if spin-polarized calculations are performed. Classical potentials, however, fail to describe the selected processes. This has been shown to have two reasons, i.e., the overestimated barrier of migration due to the artificial interaction cutoff on one hand, and on the other hand, the lack of quantum-mechanical effects which are crucial in the problem

under study. In order to get more insight on the SiC precipitation mechanism, further *ab initio* calculations are currently being performed.

[1] W. Wesch, Nucl. Instrum. Methods Phys. Res. B **116**, 305 (1996).

[2] H. Morkoç, S. Strite, G. B. Gao, M. E. Lin, B. Sverdlov, and M. Burns, J. Appl. Phys. **76**, 1363 (1994).

[3] M. A. Capano and R. J. Trew, MRS Bull. **22**, 19 (1997).

[4] G. R. Fisher and P. Barnes, Philos. Mag. B **61**, 217 (1990).

[5] J. A. Powell, D. J. Larkin, L. G. Matus, W. J. Choyke, J. L. Bradshaw, L. Henderson, M. Yoganathan, J. Yang, and P. Pirouz, Appl. Phys. Lett. **56**, 1353 (1990).

[6] A. Fissel, U. Kaiser, E. Ducke, B. Schröter, and W. Richter, J. Cryst. Growth **154**, 72 (1995).

[7] A. Fissel, B. Schröter, and W. Richter, Appl. Phys. Lett. **66**, 3182 (1995).

[8] S. Nishino, J. A. Powell, and H. A. Will, Appl. Phys. Lett. **42**, 460 (1983).

[9] S. Nishino, H. Suhara, H. Ono, and H. Matsunami, J. Appl. Phys. **61**, 4889 (1987).

[10] M. Kitabatake, M. Deguchi, and T. Hirao, J. Appl. Phys. **74**, 4438 (1993).

[11] J. A. Borders, S. T. Picraux, and W. Beezhold, Appl. Phys. Lett. **18**, 509 (1971).

[12] J. K. N. Lindner and B. Stritzker, Nucl. Instrum. Methods Phys. Res. B **147**, 249 (1999).

[13] J. K. N. Lindner, Nucl. Instrum. Methods Phys. Res. B **178**, 44 (2001).

[14] J. K. N. Lindner, Appl. Phys. A: Mater. Sci. Process. **77**, 27 (2003).

[15] P. Werner, R. Kögler, W. Skorupa, and D. Eichler, Proceedings of the 11th International Conference on Ion Implantation Technology, 1996, pp. 675–678.

[16] P. Werner, S. Eichler, G. Mariani, R. Kögler, and W. Skorupa, Appl. Phys. Lett. **70**, 252 (1997).

[17] J. K. N. Lindner and B. Stritzker, Nucl. Instrum. Methods Phys. Res. B **148**, 528 (1999).

[18] J. W. Strane, S. R. Lee, H. J. Stein, S. T. Picraux, J. K. Watanabe, and J. W. Mayer, J. Appl. Phys. **79**, 637 (1996).

[19] P. Lavéant, G. Gerth, P. Werner, and U. Gösele, Mater. Sci. Eng., B **89**, 241 (2002).

[20] F. H. Stillinger and T. A. Weber, Phys. Rev. B **31**, 5262 (1985).

[21] D. W. Brenner, Phys. Rev. B **42**, 9458 (1990).

[22] J. Tersoff, Phys. Rev. B **38**, 9902 (1988).

[23] M. Z. Bazant and E. Kaxiras, Phys. Rev. Lett. **77**, 4370 (1996).

[24] M. Z. Bazant, E. Kaxiras, and J. F. Justo, Phys. Rev. B **56**, 8542 (1997).

[25] J. F. Justo, M. Z. Bazant, E. Kaxiras, V. V. Bulatov, and S. Yip, Phys. Rev. B **58**, 2539 (1998).

[26] G. Lucas, M. Bertolus, and L. Pizzagalli, J. Phys.: Condens. Matter **22**, 035802 (2010).

[27] J. Tersoff, Phys. Rev. B **39**, 5566 (1989).

[28] F. Gao and W. J. Weber, Nucl. Instrum. Methods Phys. Res. B **191**, 487 (2002).

[29] J. Godet, L. Pizzagalli, S. Brochard, and P. Beauchamp, J. Phys.: Condens. Matter **15**, 6943 (2003).

[30] E. Holmström, A. Kuronen, and K. Nordlund, Phys. Rev. B **78**, 045202 (2008).

[31] A. Mattoni, F. Bernardini, and L. Colombo, Phys. Rev. B **66**, 195214 (2002).

[32] M. Posselt, F. Gao, and W. J. Weber, Phys. Rev. B **73**, 125206 (2006).

[33] F. Gao, W. J. Weber, M. Posselt, and V. Belko, Phys. Rev. B **69**, 245205 (2004).

[34] E. Rauls, T. Frauenheim, A. Gali, and P. Deák, Phys. Rev. B **68**, 155208 (2003).

[35] F. Gao, J. Du, E. J. Bylaska, M. Posselt, and W. J. Weber, Appl. Phys. Lett. **90**, 221915 (2007).

[36] F. Gao, E. J. Bylaska, W. J. Weber, and L. R. Corrales, Phys. Rev. B **64**, 245208 (2001).

[37] M. Bockstedte, A. Mattausch, and O. Pankratov, Phys. Rev. B **68**, 205201 (2003).

[38] A. Gali, P. Deák, E. Rauls, N. T. Son, I. G. Ivanov, F. H. C. Carlsson, E. Janzén, and W. J. Choyke, Phys. Rev. B **67**, 155203 (2003).

[39] J. Chen, P. Jung, and H. Klein, J. Nucl. Mater. **258-263**, 1803 (1998).

[40] W. J. Weber, W. Jiang, and S. Thevuthasan, Nucl. Instrum. Methods Phys. Res. B **175-177**, 26 (2001).

[41] H. Balamane, T. Halicioglu, and W. A. Tiller, Phys. Rev. B **46**, 2250 (1992).

[42] H. Huang, N. M. Ghoniem, J. K. Wong, and M. Baskes, Modell. Simul. Mater. Sci. Eng. **3**, 615 (1995).

[43] M. Tang and S. Yip, Phys. Rev. B **52**, 15150 (1995).

[44] F. Gao and W. J. Weber, Phys. Rev. B **66**, 024106 (2002).

[45] A. Mattoni, M. Ippolito, and L. Colombo, Phys. Rev. B **76**, 224103 (2007).

[46] R. Devanathan, T. D. de la Rubia, and W. J. Weber, J. Nucl. Mater. **253**, 47 (1998).

[47] K. Nordlund, N. Runeberg, and D. Sundholm, Nucl. Instrum. Methods Phys. Res. B **132**, 45 (1997).

[48] P. Erhart and K. Albe, Phys. Rev. B **71**, 035211 (2005).

[49] G. Kresse and J. Furthmüller, Comput. Mater. Sci. **6**, 15 (1996).

[50] J. P. Perdew and Y. Wang, Phys. Rev. B **33**, 8800 (1986).

[51] J. P. Perdew, J. A. Chevary, S. H. Vosko, K. A. Jackson, M. R. Pederson, D. J. Singh, and C. Fiolhais, Phys. Rev. B **46**, 6671 (1992).

[52] D. R. Hamann, M. Schlüter, and C. Chiang, Phys. Rev. Lett. **43**, 1494 (1979).

[53] D. Vanderbilt, Phys. Rev. B **41**, 7892 (1990).

[54] H. J. C. Berendsen, J. P. M. Postma, W. F. van Gunsteren, A. DiNola, and J. R. Haak, J. Chem. Phys. **81**, 3684 (1984).

[55] L. Verlet, Phys. Rev. **159**, 98 (1967).

[56] J. Tersoff, Phys. Rev. Lett. **64**, 1757 (1990).

[57] A. Dal Pino, A. M. Rappe, and J. D. Joannopoulos, Phys. Rev. B **47**, 12554 (1993).

[58] R. B. Capaz, A. Dal Pino, and J. D. Joannopoulos, Phys. Rev. B **50**, 7439 (1994).

[59] M. J. Burnard and G. G. DeLeo, Phys. Rev. B **47**, 10217 (1993).

[60] P. Leary, R. Jones, S. Öberg, and V. J. B. Torres, Phys. Rev. B **55**, 2188 (1997).

[61] G. D. Watkins and K. L. Brower, Phys. Rev. Lett. **36**, 1329 (1976).

[62] L. W. Song and G. D. Watkins, Phys. Rev. B **42**, 5759 (1990).

[63] M. Kaukonen, P. K. Sitch, G. Jungnickel, R. M. Nieminen, S. Pöykkö, D. Porezag, and Th. Frauenheim, Phys. Rev. B **57**, 9965 (1998).

[64] J. K. N. Lindner, M. Häberlen, G. Thorwarth, and B. Stritzker, Mater. Sci. Eng., C **26**, 857 (2006).

[65] A. K. Tipping and R. C. Newman, Semicond. Sci. Technol. **2**, 315 (1987).